HOKKAIDO UNIVERSITY

Title	Driving and photo-regulation of myosin-actin motors at molecular and macroscopic levels by photo-responsive high energy molecules
Author(s)	Menezes, Halley M.; Islam, Md. Jahirul; Takahashi, Masayuki; Tamaoki, Nobuyuki
Citation	Organic & biomolecular chemistry, 15(42), 8894-8903 https://doi.org/10.1039/c7ob01293d
Issue Date	2017-11-14
Doc URL	http://hdl.handle.net/2115/71967
Type	article (author version)
Additional Information	There are other files related to this item in HUSCAP. Check the above URL.
File Information	Revised_manuscript.pdf (Manuscript)

Instructions for use

Hokkaido University Collection of Scholarly and Academic Papers : HUSCAP

Driving and photo-regulation of myosin-actin motor at molecular and macroscopic level by photo-responsive high energy molecules.

Halley M. Menezes,[1,2] Md. Jahirul Islam,[1,2] Masayuki Takahashi[3] and Nobuyuki Tamaoki[1,2]*

[1]*Research Institute for Electronic Science, Hokkaido University, Kita 20, Nishi 10, Kita-Ku, Sapporo, Hokkaido, 001-0020, Japan.*

[2]*Graduate School of Life Science, Hokkaido University, Kita 10, Nishi 8, Kita-ku, Sapporo, Hokkaido, 060-0810, Japan.*

[3]*Faculty of Science, Hokkaido University, Kita 10, Nishi 8, Kita-Ku, Sapporo, Hokkaido, 060-0810, Japan*

E-mail: *tamaoki@es.hokudai.ac.jp*

Abstract

We employed azobenzene based non-nucleoside triphosphate, AzoTP, in myosin-actin motile system and demonstrated its efficiency as an energy molecule to drive and photo-regulate the myosin-actin motile function at macroscopic level along with *in-vitro* motility assay. AzoTP in its *trans* state induced the shortening of glycerinated muscle fibre whilst *cis* isomer had no significant effect. Direct photoirradiation of *cis*-AzoTP infused muscle fibre induced the shortening triggered by locally photo-generated *trans*-AzoTP in the muscle fibre. Furthermore we designed and synthesized three new derivatives of AzoTPs that served as substrates for myosin by driving and photo-regulating the myosin-actin motile function at molecular as well as macroscopic level with varied efficiency.

Introduction

Energy of nucleotide hydrolysis fuels the biomolecular motors to lug a myriad of cargos through the cytoplasm and perform a range of cellular tasks.[1,2] A purine nucleotide, adenosine triphosphate (ATP) is hydrolysed by cytoskeleton motors such as myosin, kinesin, dynein and the engendered energy is converted into mechanical work with high efficiency by undergoing conformational changes.[3-5] Harnessing these robust and versatile molecular motors for nanotechnology involves the dynamic control over their motile properties including velocity, direction of motion, processivity and on/off switching.[6-8] Light impelled modulation of ATP function is one of the pronounced approaches towards achieving the motor control.[9-11] Uncaging of inactive caged ATP by photo-irradiation (UV) to switch ON the motility from the OFF state is a remarkable study in this direction.[9] However, the irreversibility of this system made way for the development of high-efficiency reversible ATP analogues to control the motility. In recent past, our group has reported photo-sensitive ATP analogue fuels for reversible control of the motility through illumination with two different wavelengths of light.[12,13]Azobenzene based non-nucleoside triphosphate, AzoTP, in its *trans* state could drive kinesin motor, conversely, the *cis* isomer was unable to drive kinesin; thus facilitating the photo-control of gliding velocity of microtubules on immobilized kinesin between *trans* and *cis* state of AzoTP.

In-vitro motility assays provide an insight into the functioning of motor proteins on a molecular level where the motile interaction of only two isolated proteins under biochemical conditions is studied. Contrary to this, in the physiological macroscopic system motor proteins work collectively in large numbers along with other cellular components or enzymes, thus increasing the number of interacting molecules.[14-17] In our present study we explore the potential of AzoTP to photo-control such complex macroscopic system of molecular motors, hence extending its applicability over different scales. Myosin II, a muscle protein is a convenient candidate for our study since one of its chief task, muscle contraction, is studied extensively via *in-vitro* motility assay as well as muscle fibre shortening.[18-20] Myosin II ATPase translocates along actin filament and the ATP dependent cyclic sliding interaction between them powers muscle contraction as well as movement.[21,22] To substantiate this concept, glycerol extracted muscle preparation akin to living muscle was developed and evolved over the years to carry out a number of muscle contraction regulation studies.[23] Three-dimensional orderly array of myofilaments and presence of actin-associated proteins like troponin, tropomyosin render the glycerinated muscle fibre system complex than *in-vitro* motility system which involves isolated myosin and actin proteins without an orderly array. Ca^{2+} triggered regulation of glycerinated skeletal muscle fibre contractility is studied extensively.[24,25] However, regulating the contraction by photoisomerizing the substrate locally in the muscle fibre by direct irradiation isn't studied copiously.

Recently Christian Hoppmann *et al.* reported the photo-control of living skeletal muscle fibre shortening in which a photo-switchable peptide ligand inhibited the electrically stimulated fibre shortening in *cis* state whilst *trans* state had no effect on shortening.[26]

Herein, we report the AzoTP triggered driving of myosin and photo-regulation of myosin based macroscopic motile system in glycerinated skeletal muscle fibre by direct photo-irradiation of muscle fibre. *Cis* form of AzoTP fails to initiate significant shortening; following irradiation with 510nm light, the muscle fibre shortens remarkably in response to the photo-induced *trans* state. Furthermore we synthesized derivatives of AzoTP and employed them in myosin-actin motile system to investigate the correlation between the structure of substrate and its ability to perform as a photo-responsive energy molecule. We surveyed the efficiency of newly synthesized three derivatives of AzoTP to reversibly photo-control the *in-vitro* actin filament gliding velocity as well as the shortening of glycerinated muscle fibre. Amongst the newly synthesized AzoTP derivatives, the AzoTP with ether group bridging the azobenzene and triphosphate moieties performed as higher efficiency substrate for myosin motor.

Result and discussion:

Synthesis and photoisomerization of AzoTP derivatives:

The derivatives of AzoTP were synthesized by modifying the bridging group between azobenzene and triphosphate and by substitution on azobenzene moiety of previously reported parent AzoTP (**4a**). Substituting the amide linkage with ether and ethyl linkage resulted in AzoethoxyTP (**4b**) and AzoethylTP (**4d**) respectively, while the substitution of methyl groups at *meta* and *para* on azobenzene moiety resulted in DimethylAzoTP (**4c**) (Fig.1). These modifications in the parent AzoTP were done to probe the critical significance of the amide linkage in functioning of AzoTP as an energy molecule and for exploring the possibility of a further efficient azobenzene based photochromic non-nucleoside triphosphate.

Non-nucleoside triphosphate	UV PSS		Visible PSS	
	cis	*trans*	*cis*	*trans*
4a	92%	8%	38%	62%
4b	93%	7%	50%	50%
4c	93%	7%	35%	65%
4d	87%	13%	25%	75%

Table 1. Ratio of *cis* and *trans* isomers at UV and Visible photo stationary state (PSS).

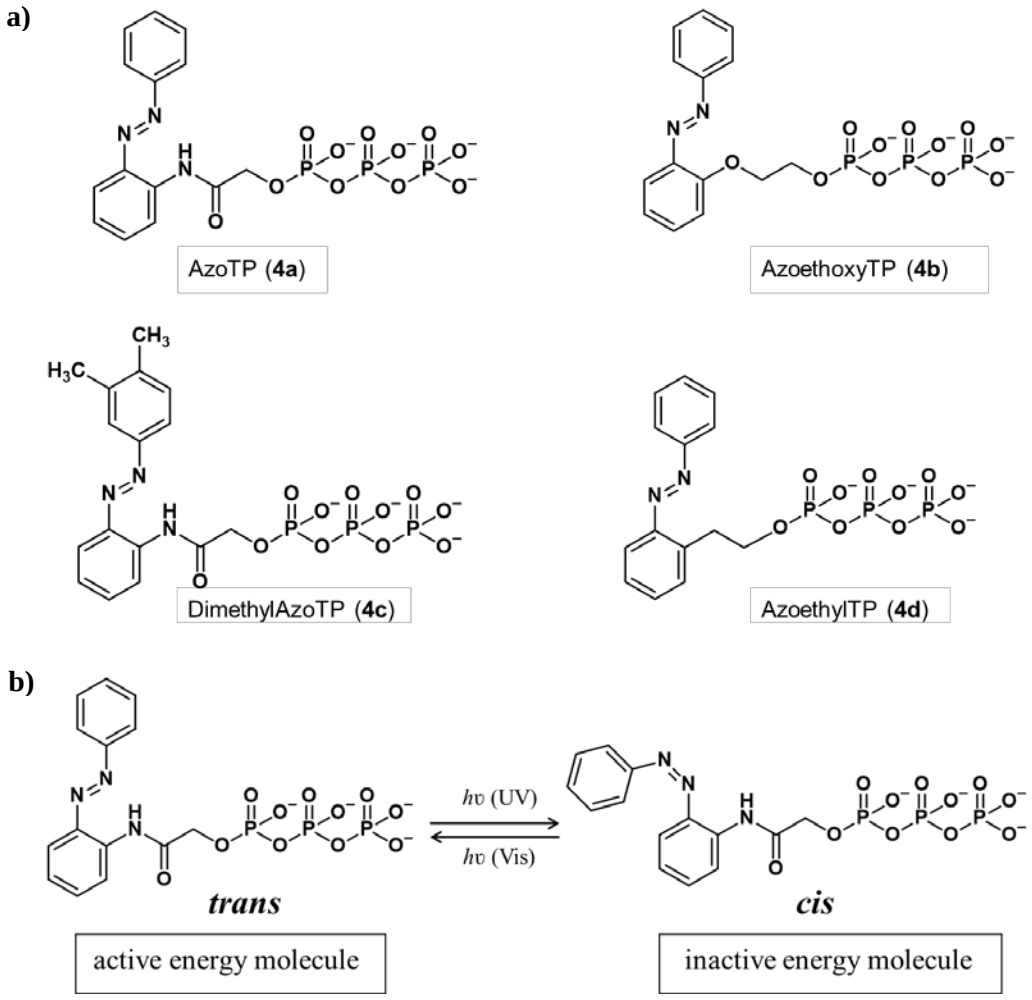

Fig.1. a) Structures of azobenzene based non-nucleoside triphosphates, AzoTP (**4a**), AzoethoxyTP (**4b**), DimethylAzoTP (**4c**) and AzoethylTP (**4d**). b) Reversible photo-isomerization of **4a**.

The reversible photoisomerization of these AzoTPs was confirmed by consecutive irradiation with 365 nm UV light and 436 nm visible light (Fig.S1). At UV photo stationary state (PSS) the AzoTPs attain their *cis*-rich state which is reversed at visible PSS resulting in thermodynamically stable *trans*-rich state. Our previous study of **4a** in kinesin-microtuble motile system suggested that *trans* isomer of **4a** was an efficient energy molecule that triggered the faster velocity of microtubules by driving kinesin motor whereas the *cis* isomer was inefficient to drive kinesin. Table 1 shows the ratio of *cis:trans* isomers of **4a**, **4b**, **4c** and **4d** at PSS induced by 365 nm and 436 nm light irradiation, determined by H^1NMR (Fig.S2). The thermal isomerization from *cis* to *trans* was evaluated by observing the changes in absorption spectra when kept in dark at room temperature. About 2% of *trans* isomer was recovered after 3h dismissing the possibility of thermal-back reactions during our experiments.

Reversible photo-control of *in-vitro* motility of myosin-actin motile system:

To assess the generalizability of **4a** to drive and control the cytoskeletal motor systems, we employed **4a** and its derivatives to myosin-actin motile system as differing from our previously reported kinesin-microtuble system. HMM (heavy meromyosin) is a soluble fragment of myosin consisting of two heads (containing nucleotide binding site and actin binding site) and a part of myosin rod; hence it was used as an ATPase motor in our *in-vitro* motility assay experiments. All the four AzoTPs tested, served as substrates for myosin by driving HMM induced gliding motility of F-actin on HMM immobilized glass surface, of which **4a** and **4b** functioned at concentrations as low as 10 µM. The average velocity of F-actin triggered by **4a**, **4b**, **4c** and **4d** are 1.25 µm/s, 1.50 µm/s, 1.24 µm/s and 0.73 µm/s respectively at saturated concentration of 0.5 mM for **4a**, **4c**, **4d** and 0.25 mM for **4b**. Photo-induced reversible control of the gliding velocity of F-actin prompted by the photo-isomerization of AzoTPs was observed as the flow cell of motility solution was irradiated with 365 nm and 436 nm light alternatingly to the PSS. The velocity decreased remarkably after irradiation with 365 nm light for 5 s corresponding to *cis*-rich state, the subsequent irradiation with 436 nm for 20 s recovered the velocity, comparable to that of initial velocity before irradiation. This phenomenon of reversible switching between the faster and slower velocity could be repeated over many cycles as represented in Fig. 2. We carried out *in-situ* photo-regulation of F-actin velocity by repeated alternating irradiation of flow cell with 365 nm UV and 510 nm visible light for 3 s and 5 s respectively captured in the 5 min long video (ESI-Mv01). Speeding actin filaments slowed down following the UV irradiation at a time interval and these slowly moving filaments recovered their speed after irradiation with 510 nm light. The magnitude of distance treaded by selected actin filaments facilitated by consecutive UV and Visible light irradiation at different time intervals is depicted in Fig. 3.

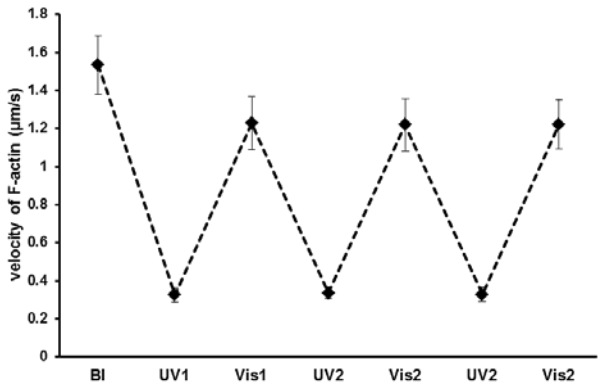

Fig. 2. Repeatability of the complete and reversible photoregulation of F-actin gliding velocity induced by **4b** **(**AzoethoxyTP) at saturated concentration (0.25 mM). (BI: before irradiation; UV: after irradiation with 365 nm light; Vis: after irradiation with 436 nm light). Error bars: standard deviation for 10 actin filaments.

The change in velocity between the two photoisomerized states of AzoTP molecules is 54%, 79%, 81%, 80% for **4a**, **4b**, **4c**, **4d** respectively at saturated concentrations. However, at 0.1mM concentration the magnitude of switching is higher for all AzoTPs as the difference in velocity is about 87 – 90%. The gliding velocities fuelled by AzoTPs in their *trans* state (black solid circles) and *cis*-rich state (blue solid circles) with respect to the range of concentrations are shown in Fig.4.

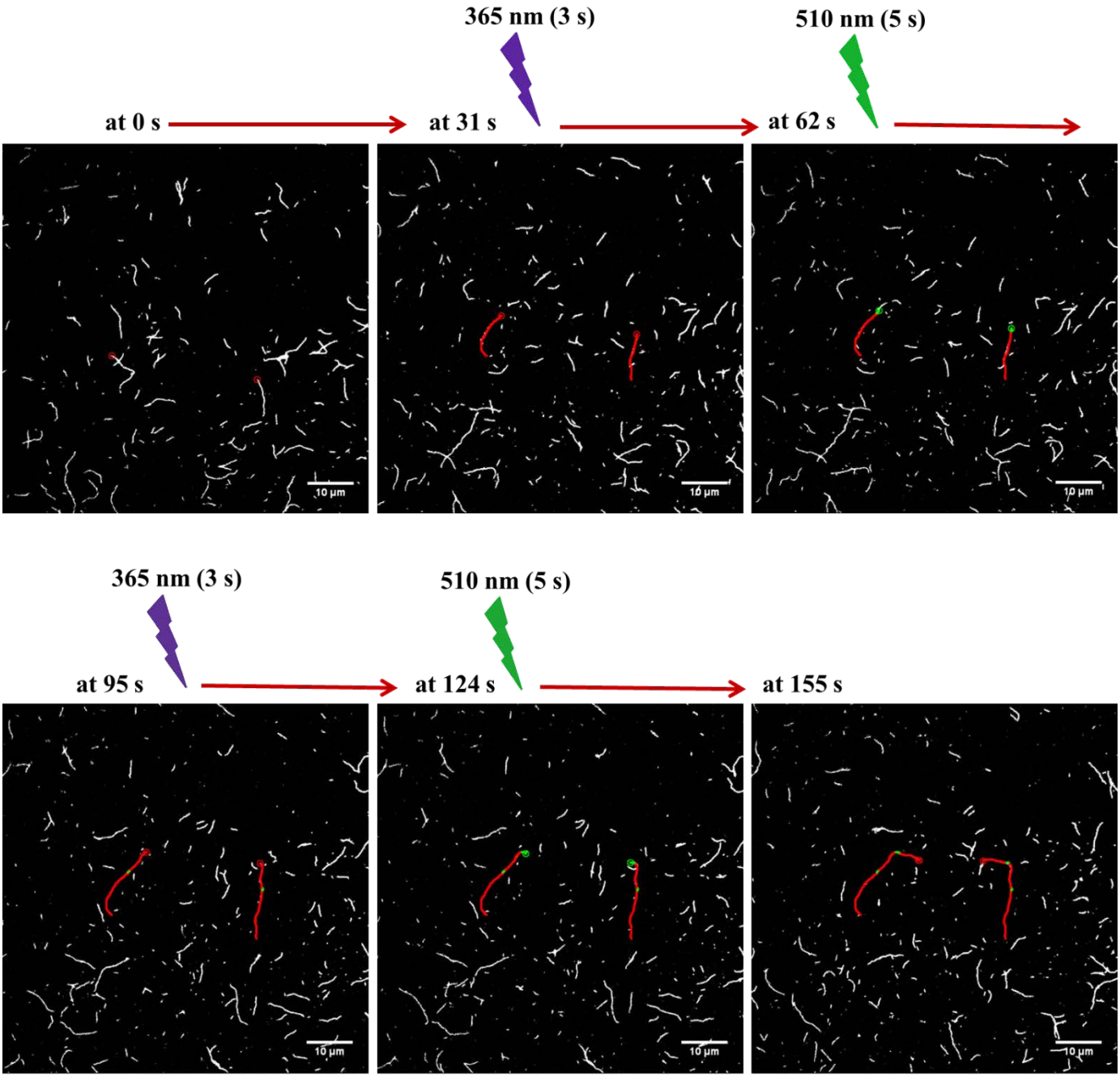

Fig. 3. Fluorescence images of F-actin motility driven by *trans* and *cis* state of **4a** (40 µM) by *in-situ* photo-regulation experiment with alternating irradiation at 365 nm (3 s) and 510 nm (5 s). The distance moved by two actin filaments is indicated in lines by tracking the path of filament heads; red circles denote the position of actin filament heads before irradiation (*trans* state), green and red lines denote the distance treaded by F- actin after UV (365 nm) and Vis (510 nm) irradiations respectively.

Concentration dependent velocity of actin filaments obeys the Michaelis-Menten equation and the obtained apparent K_m (K_{app}) values indicate that the apparent binding affinity of AzoTP for myosin ($1/K_{app}$ = 9.9 mM^{-1}) is twenty five times higher than that for kinesin motor ($1/K_{app}$ = 0.4 mM^{-1}) (as obtained in our previous work). The maximum gliding velocity (V_{max}) of F-actin induced by **4a**, **4b**, **4c** and **4d** are 1.5 µm/s, 1.9 µm/s, 1.7 µm/s and 1.0 µm/s respectively, which are 53%, 68%, 59% and 35% of that of ATP (V_{max} = 2.9 µm/s) at saturated concentration. Our previous report on AzoTP explained that the microtubule velocity driven by *cis*-rich state of AzoTP is due to the remaining *trans* at *cis*-rich PSS, which corresponded to 8%. In our current study too we plotted a theoretical curve corresponding to remaining *trans* of all the four AzoTP molecules at their respective *cis*-rich PSS to validate this explanation. Fig.4 shows the Michaelis-Menten plot for concentration dependent velocity of all four AzoTPs and theoretical curve (red lines) for remaining *trans* amounting for 8%, 7%, 7% and 13% (table 1) in *cis*-rich state of **4a**, **4b**, **4c** and **4d** respectively. These observations insinuate that AzoTPs in their *cis* state intrinsically have no ability to function as energy molecules to drive the motor proteins.

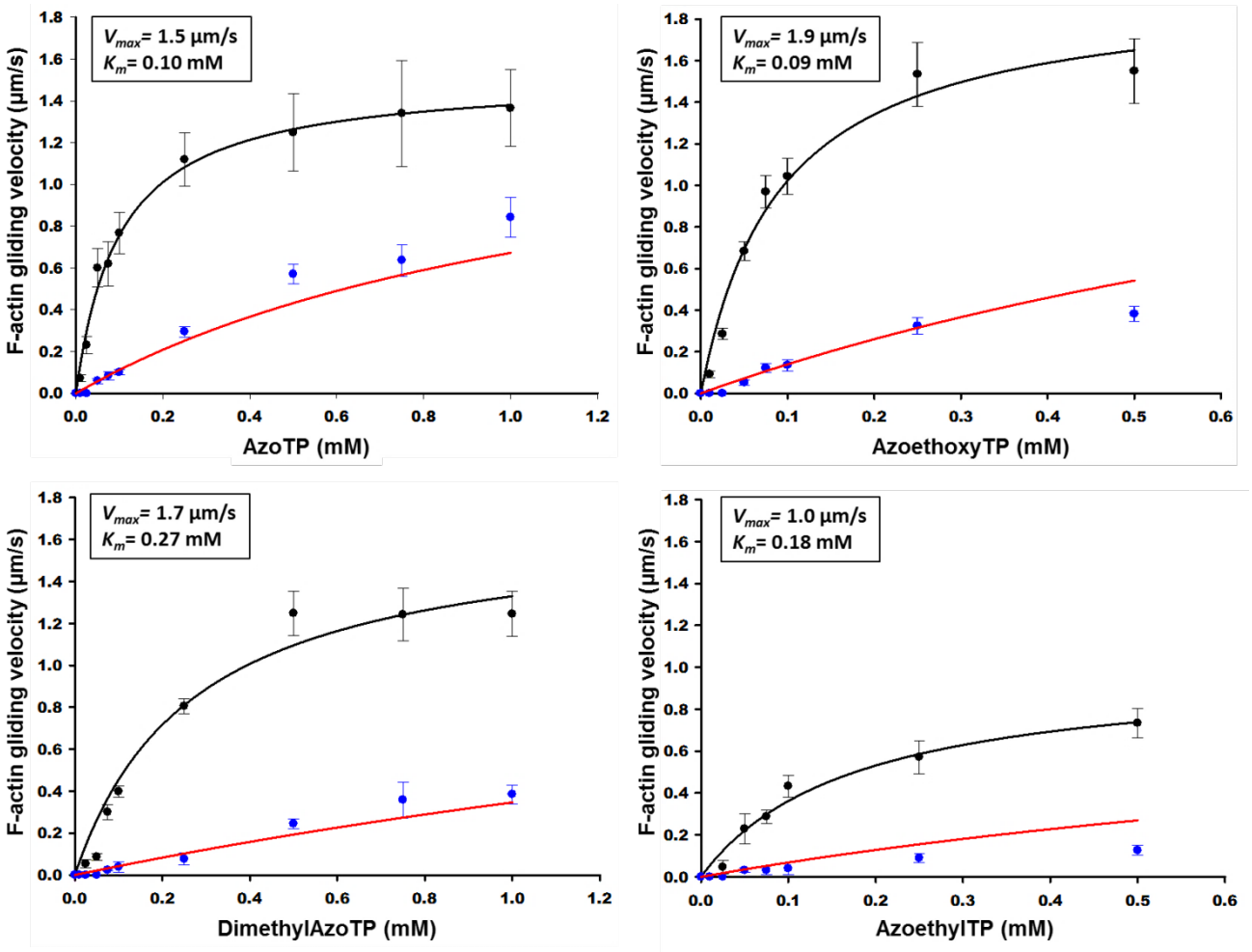

Fig. 4. Gliding velocity of actin filaments as a function of AzoTPs concentration. (Black solid circles: velocities before irradiation; black line: curve fitted using Michaelis–Menten equation; Blue circles: velocities after irradiating at 365 nm;

red line: theoretical curve derived from the black line for remaining *trans* in the *cis*-rich state.) Error bars: standard deviations for 10 actin filaments.

Although the K_{app} of **4a** and **4b** is almost threefold less than **4c**, the V_{max} of these three AzoTPs is comparable, since all three K_{app} were in submillimolar range. However, **4d** has considerably lower V_{max}, though its K_{app} is in the same range as that of **4a**, **4b** and **4c**. These results imply that the substrates **4b** and **4a** bind to the myosin motor with higher affinity than that of **4c** and **4d**. Structural studies of chicken skeletal myosin subfragment 1 revealed that the nucleotide binding pocket is formed by the residues from the N-terminal, central, and C-terminal sections of myosin motor head domain.[27,28] The adenine binding pocket is formed by amino acid residues Phe^{129}-Tyr^{135} and Glu^{187}-Lys^{191} contributed by the N-terminal segment as seen in the X-ray structural studies of *Dictyostelium discoideum* myosin II complex (S1dC.MgADP.BeF$_x$).[29] Despite the presence of several water molecules with the potentiality for hydrogen bonding, very few specific interactions were seen between the adenine base and myosin heavy chain except the hydrogen bond between N6 of adenine and sidechain of Tyr^{135}. This is in line with the observations that myosin utilizes a wide range of nucleotides and organic triphosphates,[30,31] thus substantiating the functionality of our AzoTP molecules as substrates for myosin. Also the ribose moiety which bridges the adenine and triphosphate moieties forms very few interactions with the protein, enabling the myosin to utilize nucleotides and organic triphosphates with ribose ring replaced by variety of functional groups. However, ribose ring oxygen, 04' forms a hydrogen bond with Asn^{127} sidechain.[29] Comparing the chemical structures of our AzoTP molecules with that of ATP suggests that the linker groups (ether, amide, ethyl) might fulfil the role of ribose and azobenzene takes adenine's place. This presumption provides an insight into the varied binding affinity of our four AzoTP substrates as well as their *cis* and *trans* isomers. Higher binding affinity of **4b** ($1/K_{app}$ = 11.0 mM^{-1}) could be attributed to the ether group bridging the triphosphate moiety and azobenzene, where the oxygen of ether forms a hydrogen bond with the side chain of Asn^{127}, analogous to the ribose oxygen of ATP.[29] Similarly the carbonyl oxygen of amide group in **4a** could participate in the hydrogen bonding by acting as a hydrogen acceptor. Absence of any potential hydrogen bond forming atoms in the bridging ethyl group elicits the lower binding affinity ($1/K_{app}$= 5.7 mM^{-1}) in **4d** than **4a** and **4b**. Although there is carbonyl oxygen in **4c** with the potentiality for hydrogen bond formation, yet the binding affinity ($1/K_{app}$ = 3.7 mM^{-1}) is almost three fold lower than **4a** and **4b**. We assume this weaker binding affinity is resulted by the bulkiness of the substrate due to the presence of two methyl substituents on azobenzene moiety which might sterically interfere in the binding of substrate and myosin. AzoTPs in their *cis* state show no intrinsic ability as substrates for myosin unlike the active *trans* state. It is well established that the isomerization of azobenzene from *trans* to *cis* changes the geometry from flat to bent or round shape resulting in bulkiness. We surmise that the inability of *cis* isomer to bind

in the nucleotide binding pocket could be ascribed to its bulkiness. In addition the adenine binding site is relatively hydrophobic[32,33] thus the hydrophilic *cis* isomer isn't favoured.

Photo induced regulation of macroscopic motile system of myosin motor:

As an approach to probe the efficiency of AzoTPs at macroscopic level to drive and control the motile functions, we conducted the simple glycerinated muscle fibre shortening experiments where the extent of shortening was assessed by unaided eye. The fibres used were of ~ 0.5 mm thickness and 7- 8 mm in length. First we tested our parent AzoTP molecule **4a** for macroscopic studies. **4a** in its *trans* state induced the shortening of muscle fibre accounting for 40 – 45% shortening of muscle fibre's initial length. Pre-generated *cis* isomer of **4a** didn't induce any significant shortening, thus affirming the poor activity of **4a** in its *cis*-form as evidenced in our molecular *in-vitro* motility experiments (Fig.5a, ESI-Mv02). When the *cis* isomer infused muscle fibre was irradiated with 510 nm light for 10 s, remarkable shortening of about 40% of its initial length was observed, thus confirming the efficiency of **4a** to drive and photocontrol the myosin motor function in the macroscopic system (Fig.5b, ESI-Mv04). To corroborate that the shortening was resulted by the photoisomerization of **4a** and not by the thermal energy of illumination, we irradiated the muscle fibre infused in buffer solution without **4a** at 510 nm, which exhibited no shortening (ESI-Mv03).

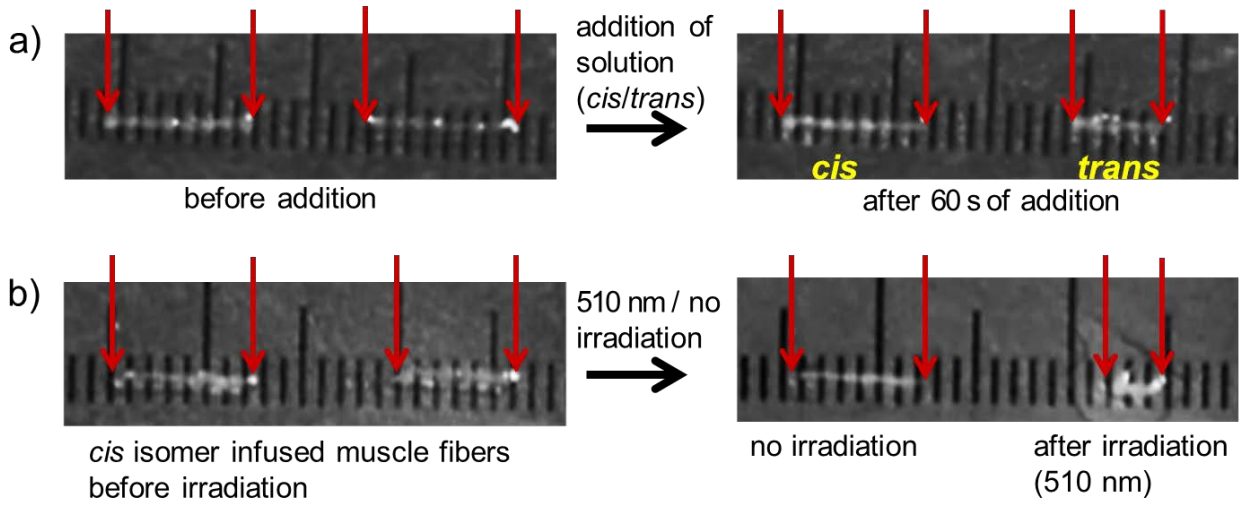

Fig. 5. Non-nucleoside triphosphate **4a** induces and photo-controls the shortening of glycerinated muscle fibre. a) buffer solution with *trans*-**4a** (3 mM) induces shortening while *cis*-**4a** has no significant effect on shortening. b) *cis*-**4a** infused muscle fibre shortens after irradiation with 510 nm light, no significant change in length in non-irradiated fibre. Red arrows point at the two edges of the fibre. The scale seen in the photographs is 1 mm.

Further, the ability of all three newly synthesized AzoTPs to initiate and photo-control the shortening was investigated. Fig. 6 represents the percentage change in muscle fibre length with respect to time, induced by all the four AzoTPs at 3 mM (total). Shortening of muscle fibre with respect to time

increases with the order of **4a**~ **4b** > **4c** > **4d**, where the substrates **4a** and **4b** induce the shortening swiftly with evidently larger magnitude of length change than **4c** and **4d** over the time range. Similar to **4a**, the *cis*-form of energy molecules **4b**, **4c** and **4d** was unable to induce any significant shortening and the 510 nm light irradiation of *cis* infused muscle fibres induces the shortening except **4d**. Experiments involving the **4a** concentration dependent shortening rate showed that there is no significant change in muscle length below 0.5 mM of *trans*-**4a** (Fig. S3). This explains the no significant shortening induced by *cis*-rich state of **4a** at 3 mM (total) despite the presence of expected 8% (0.25 mM) of remained *trans*. The order of performance of four AzoTP substrates (**4a**~ **4b** > **4c** > **4d**) in macroscopic system is consistent with the K_{app} values obtained by the molecular level studies. Unlike the molecular *in-vitro* motility system, the glycerinated muscle fibre system involves the ordered array of myofibrils which could furnish the steric hindrance, but the AzoTPs efficiently replicated the photo-regulation of motor function in the glycerinated muscle fibre as well. AzoTP energy molecules photo-regulate the muscle fibre shortening by photoisomerizing to active *trans* state from inactive *cis* state locally in the muscle fibre by direct photo-irradiation.

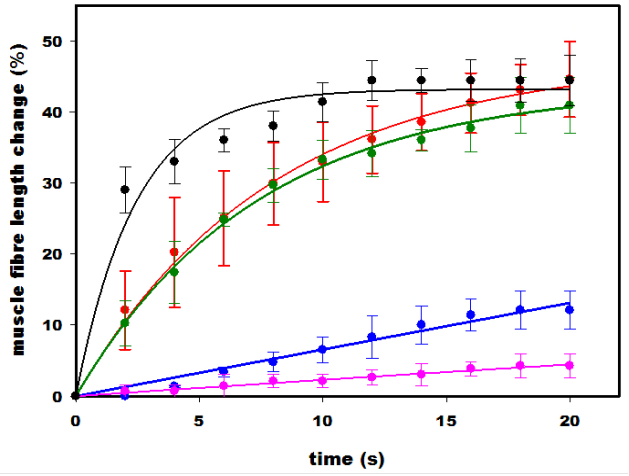

Fig. 6. Muscle fibre length change ($L_{(t=0)}$ - $L_{(t)}$ / $L_{(t=0)}$) with respect to the time for AzoTPs (3 mM) **4a**, **4b**, **4c** and **4d** induced fibre shortening. Black, red, green, blue and pink circles represent the % length change induced by ATP, **4a, 4b, 4c and 4d** respectively; the lines are best-fit through the data trend. Error bars: standard deviation for 4 fibres.

Conclusion

In a step towards employing our AzoTP energy molecules to regulate the macroscopic systems, we have demonstrated the photo-regulated initiation of shortening in glycerinated skeletal muscle fibre induced by the photoisomerization. Direct irradiation with visible light initiated the shortening in the inactive *cis*-AzoTPs infused muscle fibre by locally photo-generated *trans*-AzoTPs. The *trans* form of AzoTPs initiates the contraction and shortens the muscle fibre to almost half of its initial length, whilst *cis* isomer's contribution is insignificant. Also, we demonstrated the functionality of **4a** as an

efficient substrate for myosin motor in addition to kinesin as reported previously, thus implying its generalizability for cytoskeletal motors. The newly designed and synthesized three AzoTPs serve as the substrate for myosin motor and photoregulate the motility at molecular as well as macroscopic level. All the four AzoTP molecules drive myosin triggered *in-vitro* gliding velocity of F-actin with 50 to 60% efficiency of that obtained with ATP and photo-control the velocity between fast/slow states by undergoing photoisomerization. Our demonstration of the photocontrol of macroscopic glycerinated muscle fibre system is a promising indication towards regulating the much complex intact *in vivo* systems and organisms by utilizing photoresponsive energy molecules. The regulation of complex biological systems could benefit in investigating the disorders and targeted drug delivery. Efficient functionality of our AzoTP molecules in myosin-actin and kinesin-microtubule motile system at molecular as well as macroscopic level makes them interesting photoswitches which could find potential in various biomolecular tasks.

Experimental

Instrumentation

^{1}H, ^{13}C and ^{31}P NMR spectra were recorded using ECX-400 (400 MHz) spectrometer (JEOL). Analysis of the AzoTPs was carried out in a Shimadzu reversed-phase (RP) HPLC system. An EYELA FDU-2200 lyophilisation system was used for freeze-drying. Electrospray ionization time-of-flight Mass Spectrometry (ESI-TOF MS) was performed using a JMS-T100CS instrument (JEOL) operated in the negative-ion mode. High-resolution mass spectrometry was measured on a Thermo Scientific Exactive mass spectrometer with Electrospray Ionization (ESI). Column chromatography was performed using silica gel 60 N (neutral, 60-120 µm, Kanto chemicals). Thin layer chromatography (TLC) was carried out on precoated silica gel 60 F_{254} aluminium sheets (Merck). UV-Vis absorption spectra were recorded using an Agilent 8453 single-beam spectrophotometer and a Shimadzu UV-1800 absorption spectrophotometer. A mercury lamp (Ushio) with band pass filters for 436 and a Hamamatsu LED Controller (model C11924-101) for 365 nm light was used for photoisomerization and *in-vitro* motility experiments. Hayasaka LED Controller (model CS_LED 3W_510) for 510 nm light was used for photoregulation of *in-situ* motility and muscle fibre shortening experiments. An inverted fluorescence optical microscope (Olympus IX71) equipped with a UPlan F1 100×/1.30 oil C1 objective lens (Olympus) was used for the motility experiments in conjunction with appropriate filters (640 nm excitation filter). An EMCCD digital camera (Andor Solis Technology, model DL-604M-0EM-H1) was used to record videos.

Chemicals

All chemical and biochemical reagents were purchased from commercial sources (Tokyo Chemical Industry; Watanabe Chemical Industries; Wako Pure Chemical Industries; Dojindo Molecular Technologies) and used without purification.

Protein preparation

All experiments were performed in compliance with the relevant laws and institutional (Hokkaido University, Japan) guidelines. Skeletal muscle myosin was prepared from chicken pectoralis muscle according to the literature and was stored at -20^{o}C in 50% glycerol from which the HMM was prepared on the next day.[34] HMM was produced by α-chymotrypsin digestion of myosin for 10 min at 25^{o}C, followed by dialysis and aliquots were quickly frozen in liquid N_2 and stored at -80^{o}C.[34] F-actin was prepared from rabbit skeletal muscle as described by Pardee and Spudich[35] and then labelled with phalloidin -CF™633 dye conjugate (Biotium) for performing *in-vitro* motility assays. Concentration of proteins was determined by measuring absorption at 280 nm with extinction coefficients of 0.63 and 1.1 for HMM and actin respectively. The purity of proteins was confirmed by SDS-PAGE.

In-vitro motility assay

Flow cell preparation and motility assay techniques were followed according to the literature.[18,19,36] Gliding velocities were measured with ImageJ plugin MTrackJ.[37] Average of velocity of 10 filaments was determined in each experiment. All the assays were performed at 23.5^{o}C. The motility solution consisted of 100 mM HEPES (pH 7.4), 25 mM NaCl, 4 mM $MgCl_2$, 1 mM EGTA, 10 mM DTT, 0.5 mg/ml BSA and a 20 mM glucose, 20 µg/ml catalase, 0.1 mg/ml glucose oxidase. Calculated ironic strength was 38 mM. The flow cell was directly irradiated with 365 nm (LED) light for 5 s and with 436 nm (Hg lamp) for 20 s alternatingly.

Muscle fibre preparation and shortening experiments

The chicken skeletal muscle stripes were prepared by glycerol extraction method and stored at -20^{o}C in 50% glycerol-buffer.[20,38] Transferred to a 20% glycerol-buffer solution 20 min before conducting the experiment and then transferred to the buffer solution without ATP/AzoTP 3 min before starting the experiment. The buffer consisted of 137 mM NaCl, 2.7 mM KCl, 10 mM Na_2HPO_4 and 1.8 mM KH_2PO_4 ; pH 7.4 The muscle stripe was teased into ~0.5 mm thick and 7 mm-8 mm long fibres which were then mounted on the glass slide and the buffer solution containing AzoTPs (4 µL) was added. The changes in the length were observed by unaided eyes and analysed the change in length by recording the video for shortening process using a Canon digital camera. The length change vs

time was measured by dividing the net change in the length of the fibre with respect to its initial length at a time interval by the initial length ($L_{(t=0)}$-$L_{(t)}$ / $L_{(t=0)}$). For the photo-regulation experiments, the muscle fibres mounted on the slide were directly irradiated with 510 nm (LED) light after adding the buffer solution containing *cis*-rich state AzoTP substrates.

Synthesis of new derivatives of AzoTP

Photochromic non-nucleoside triphosphate **4a** was synthesized as reported in our previous report.[13] The general synthetic route for AzoTP molecules involves two major steps: step 1) synthesis of hydroxyl attached functional group tethered azobenzene; 2) Phosphorylation of this functionalized azobenzene to obtain azobenzene based triphosphate. The new derivatives of AzoTP, **4b** and **4d** were synthesized by functionalizing azobenzene with ethoxy and ethyl groups; likewise **4c** was synthesized by functionalizing dimethyl substituted azobenzene with amide group as represented in scheme 1. Detailed synthetic scheme of all the three derivatives is presented in ESI.

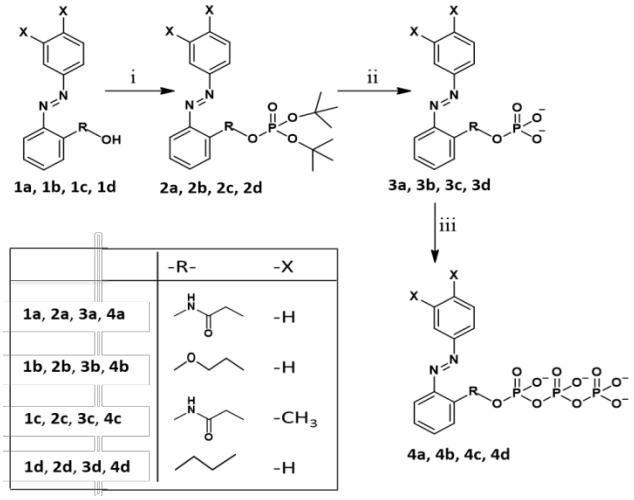

Scheme 1. General synthetic route for AzoTP molecules. Reaction conditions; **i**) di-*tert*-butyl *N*,*N*-diisopropylphosphoramidite, 1*H*-tetrazole, dry THF, Ar atmosphere, RT, 6h and then mCPBA, 0°C, 1h followed by RT, 40 min; **ii)** Trifluoroacetic acid, dry CH_2Cl_2, Ar atmosphere, RT, 6 h; **iii**) Tributylamine, carbonyldiimidazole, pyrophosphate, dry DMF, Ar atmosphere, RT, overnight.

Synthesis of **1b**: Azobenzene (1.0 g, 5.49 mmol), $Pd(OAc)_2$ (0.123 g, 0.549 mmol), $PhI(OAc)_2$ (3.536 g, 10.98 mmol), AcOH (6.3 ml, 109.8 mmol) were all added to ethylene glycol (22 ml) in a RB flask and heated at 80^{o}C for 24 h. AcOH was removed by rotary evaporation and the reaction mixture was partitioned between organic (EtOAc) and aqueous layer. The organic phase was dried over $MgSO_4$ and concentrated in a rotary evaporator and the purified compound obtained through column chromatography (SiO_2, Hexane/EtOAc 7:3). Dark red crystals of **1b** were obtained (1.03 g, 77%). R_f = 0.33 (Hexane/EtOAc 7:3). Mp: 74.5- 76 °C; ^{1}H NMR [400MHz, $CDCl_3$]: δ 7.88 (dd, J_1 =

8.3 Hz, J_2 = 2.7 Hz, 2H), 7.69 (dd, J_1 = 8.1 Hz, J_2 = 1.7 Hz, 1H), 7.43-7.52 (m, 4H), 7.18-7.1 (m, 2H), 4.34 (t, J = 4.4 Hz, 2H), 3.96 (q, J = 6.4 Hz, 2H), 3.09 (t, J = 6.5 Hz, 1H). ^{13}C NMR [100.5 MHz, $CDCl_3$] δ = 156.10, 153.00, 143.42, 132.64, 131.18, 129.26, 122.97, 122.24, 118.00, 116.76, 72.55, 61.19. HRMS (ESI, m/z) calculated for $C_{14}H_{16}N_2O_2Na$ $[M + Na]^+$: 265.09475; found: 265.09473 (observed error of -0.07 ppm is within the range of instrumental error of ±5.00 ppm).

1c was synthesized via three steps via **5** and **6** (scheme 2).

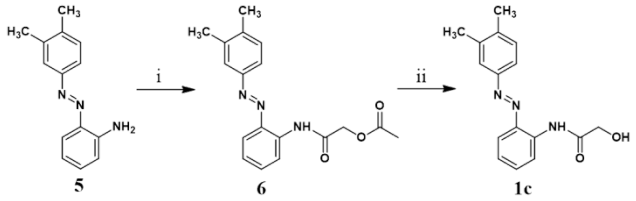

5 6 1c

Scheme 2. Synthetic route for **1c**; Reaction conditions: **i**) Acetoxyactyl chloride, Triethylamine, DCM, RT, 3h; **ii**) K_2CO_3, MeOH, RT, Overnight.

Synthesis of **5**: *m*-CPBA (9.40 g, 60.02 mmol) was added to a solution of 3,4-dimethylaniline (3.64 g, 30 mmol) in EtOAc (300 mL) at 0°C in an ice bath. The reaction mixture was stirred for 3 h and extracted with EtOAc and saturated $NaHCO_3$ then washed with water. Organic phase was dried with $MgSO_4$ and then reduced the volume using a *rotovap*. When the volume was reached to approx. 150 mL, the evaporation was stopped and the solution was degassed with dry N_2 for 15 min. 1,2-phenylenediamine (3.2 g, 30 mmol) and acetic acid (1mL) were added to this solution under N_2-atmosphere. The reaction mixture was stirred at 50 °C for 89 h. After 89 h the reaction mixture was extracted with water and EtOAc. The organic part was dried with $MgSO_4$ and concentrated in a *rotovap*. The residue was purified by silica gel column chromatography. The compound was eluted with hexane/EtOAc, 9:1 to afford the dark red crystals of **5** (2.70 g, 40%). R_f = 0.30 (Hexane/EtOAc 9:1).Mp: 128-130 °C. ^{1}H NMR [400MHz, $CDCl_3$] δ 7.80 (dd, J = 8.1, 1.5 Hz, 1H), 7.63 – 7.58 (m, 2H), 7.25 – 7.17 (m, 2H), 6.81 (ddd, J = 8.2, 7.1, 1.3 Hz, 1H), 6.76 (dd, J = 8.2, 1.1 Hz, 1H), 5.83 (br, 2H), 2.35 (s,3H), 2.33 (s, 3H). ^{13}C NMR [100.5 MHz, $CDCl_3$] δ 151.42, 142.99, 139.27, 137.46, 137.26, 131.94, 130.34, 127.27, 123.14, 120.10, 117.49, 117.06, 20.03, 19.92. HRMS (ESI, m/z) calculated for $C_{14}H_{16}N_3$ $[M + H]^+$: 226.13387; found: 226.13383 (observed error of -0.19 ppm is within the range of instrumental error of ±5.00 ppm).

Synthesis of **6**: Triethylamine (2.54 mL, 18.15 mmol) was added to a solution of **5** (2.70 g, 12.10 mmol) in DCM (90 mL) at 0°C in an ice bath. While stirring, acetoxyactyl chloride (1.95 mL, 18.15 mmol) was added dropwise to the reaction mixture at 0°C in an ice bath. Then the reaction mixture was kept in ice bath for 15 min followed by 3 h at room temperature. The reaction mixture was extracted with DCM and water. The organic part was dried with $MgSO_4$ and all the solvents were removed using the *rotovap*. The residue was purified by washing with hexane several times and with DCM twice, then finally dried under vacuum to afford 3.51 g (89%) of orange solid of **6**. R_f = 0.1

(Hexane/EtOAc 9:1).Mp 148-149 °C. ^{1}H NMR (400 MHz, DMSO-D6) δ 10.23 (s, 1H), 8.32 (dd, *J* = 8.3, 1.1 Hz, 1H), 7.82 – 7.71 (m, 3H), 7.56 – 7.52 (m, 1H), 7.38 (d, *J* = 8.1 Hz, 1H), 7.28 – 7.24 (m, 1H), 4.81 (s, 2H), 2.35 (s, 3H), 2.33 (s, 3H), 2.15 (s, 3H). ^{13}C NMR [100.5 MHz, DMSO-D6] δ 169.74, 165.85, 150.57, 141.03, 140.70, 137.55, 136.00, 132.25, 130.35, 124.41, 124.20, 121.79, 120.47, 116.42, 63.00, 20.53, 19.54, 19.45. HRMS (ESI, m/z) calculated for $C_{18}H_{19}N_3O_3Na$ [M + Na]$^{+}$: 348.13186; found: 348.13154 (observed error of -0.93 ppm is within the range of instrumental error of ±5.00 ppm).

Synthesis of **1c** : K_2CO_3 (2.79 g, 20.0 mmol) was added to a solution of **6** (3.48 g, 10.69 mmol) in MeOH/DMSO (40mL+10mL) at room temperature. The reaction mixture was stirred for overnight. Then the reaction mixture was partitioned between EtOAc and water. The EtOAc part was dried with $MgSO_4$ and all the solvents were removed using a *rotovap*. The residue was washed with hexane several times and with DCM twice and finally dried under vacuum to afford orange solid of compound **1c** (2.91 g, 96%). R_f = 0.13 (Hexane/EtOAc 7:3).Mp 170-172 °C. ^{1}H NMR (400 MHz, DMSO-D6) δ 11.10 (s, 1H), 8.64 (dd, *J* = 8.4, 1.1 Hz, 1H), 7.82 – 7.77 (m, 2H), 7.71 (dd, *J* = 8.0, 2.0 Hz, 1H), 7.58 – 7.53 (m, 1H), 7.39 (d, *J* = 8.0 Hz, 1H), 7.27 – 7.23 (m, 1H), 6.40 (s, 1H), 4.09 (s, 2H), 2.34 (s, 3H), 2.33 (s, 3H). ^{13}C NMR [100.5 MHz, DMSO-D6] δ 170.99, 150.42, 141.22, 138.78, 137.73, 135.46, 132.77, 130.53, 123.65, 123.26, 120.67, 119.42, 118.95, 61.98, 19.59, 19.56. HRMS (ESI, m/z) calculated for $C_{16}H_{17}N_3O_2Na$ [M + Na]$^{+}$: 306.12130; found: 306.12127 (observed error of -0.09 ppm is within the range of instrumental error of ±5.00 ppm).

Synthesis of **1d**: A solution of 2-(2-aminophenyl)ethanol (4.65 g, 33.90 mmol) in toluene (200 mL) was degassed under a stream of N_2 for 15 min then nitrosobenzene (3.63 g, 33.89 mmol) and acetic acid (0.8 mL) were added under Ar-atmosphere. The reaction mixture was stirred at 60 °C for 72h. The solvent of the reaction mixture was evaporated in *rotovap* and partitioned between water and CH_2Cl_2 (DCM). The DCM part was dried (with $MgSO_4$) and concentrated in a *rotovap*. The residue was purified by column chromatography (SiO_2, Hexane/EtOAc 6:4) to afford dark red viscous liquid of **1d** (5.75 g, 75%). R_f = 0.30 (Hexane/EtOAc 7:3).^{1}H NMR [400MHz, $CDCl_3$]: δ 7.91 – 7.88 (m, 2H), 7.71 (dd, , J_1 = 8.0 Hz, J_2 = 1.0 Hz, 1H), 7.55 – 7.45 (m, 3H), 7.44 – 7.39 (m, 2H), 7.37 – 7.33 (m, 1H), 3.96 (dd, J_1 = 12.2 Hz, J_2 = 6.4 Hz, 2H), 3.40 (t, *J* = 6.4 Hz, 2H), 2.02 (t, *J* = 5.6 Hz, 1H). ^{13}C NMR [100.5 MHz, $CDCl_3$] δ 152.72, 150.55, 138.70, 131.34, 131.23, 131.08, 129.14, 127.29, 122.94, 115.72, 63.87, 35.09. HRMS (ESI, m/z) calculated for $C_{14}H_{14}N_2ONa$ [M + Na]$^{+}$: 249.09983; found: 249.09957 (observed error of -1.06 ppm is within the range of instrumental error of ±5.00 ppm).

General synthetic procedure for phosphorylation (step 2):

A) Monophosphate formation: 1*H*-Tetrazole (3 eq.) was added to a solution of **1a-d** (1 eq.) and di-*tert*-butyl *N*,*N*-diisopropylphosphoramidite (1.3 eq.) in dry THF. This reaction mixture was stirred

for 6 h at room temperature. A solution of mCPBA (65%, 1.7 eq.) in dry CH_2Cl_2 was added and stirred for 1h in an ice bath followed by stirring at room temperature for 25 min. Saturated aqueous $NaHCO_3$ was added and the mixture was stirred further for 40 min. The reaction mixture was extracted in an organic (EtOAc) and aqueous solution (NaCl). The organic phase separated, dried over $MgSO_4$ and concentrated in a rotary evaporator, passed through column chromatography to obtain the purified *tert*-butyl protected monophosphates **2a-d**. Trifluoroacetic acid (16 eq.) was added to the solution of this protected monophosphate (1 eq.) in dry CH_2Cl_2 and stirred for 6 h at room temperature followed by solvent evaporation. For the complete removal of CF_3COOH, the procedure of addition of MeOH and evaporation was repeated thrice followed by CH_2Cl_2 wash. Vacuum dried the obtained residue of monophosphate (**3a-d**) and dissolved in water by adjusting the pH to 7.5 using 1M NaOH. This solution was eluted through a DEAE Sephadex A-25 column with 0.5M triethylammonium hydrogencarbonate solution at 4 °C to convert the monophosphate into its triethylammonium salt. Triethyl ammonium hydrogencarbonate was removed by evaporation with EtOH several times.

2b: Reddish orange viscous liquid. Yield = 0.15 g (14%). R_f = 0.10 (Hexane/EtOAc 7:3). ^{1}H NMR (400 MHz, $CDCl_3$): δ 8.6 (br, 1H), 7.91 (d, *J* = 8.0 Hz, 2H), 7.65 (d, *J* = 8.0 Hz, 1H), 7.52−7.40 (m, 4H), 7.12 (d, *J* = 8.2 Hz 1H), 7.05 (t, *J* = 7.6 Hz, 1H), 4.43 – 4.37 (m, 4H), 1.46 (s, 18 H). ^{13}C NMR [100.5 MHz, $CDCl_3$] δ 156.22, 153.07, 142.88, 132.38, 130.89, 129.05, 123.12, 121.64, 117.13, 115.34, 82.66 (d, *J* = 7.4 Hz), 68.99(d, *J* = 8.5 Hz), 64.95 (d, *J* = 6.0 Hz), 29.88 (d, *J* = 4.3 Hz). HRMS (ESI, m/z) calculated for $C_{22}H_{31}N_2O_5PNa$ $[M + Na]^+$: 457.18628; found: 457.18634 (observed error of 0.13 ppm is within the range of instrumental error of ±5.00 ppm).

2c: Orange solid. Yield = 1.54 g (42%). R_f = 0.25 (Hexane/EtOAc 7:3). Mp: 132-133 °C. ^{1}H NMR (400 MHz, $CDCl_3$): δ = 10.71 (s, 1H), 8.69 (dd, J_1 = 8.4 Hz, J_2= 1.2 Hz, 1H), 7.87 – 7.80 (m, 3H), 7.49 – 7.45 (m, 1H), 7.31 (d, *J* = 7.8 Hz, 1H), 7.23 – 7.18 (m, 1H), 4.60 (d, *J* = 7.0 Hz, 2H), 2.41 (s, 3H), 2.35 (s, 3H), 1.46 (s, 18H). ^{13}C NMR [100.5 MHz, $CDCl_3$] δ 166.16 (d, *J* = 8.9 Hz), 150.95, 141.13, 139.82, 137.72, 135.50, 132.30, 130.64, 125.38, 124.21, 120.27, 120.30, 118.56, 83.64 (d, *J* = 7.1 Hz), 65.72 (d, *J* = 6.7 Hz), 29.92 (d, *J* = 4.2 Hz), 20.04, 19.90. HRMS (ESI, m/z) calculated for $C_{24}H_{34}N_3O_5PNa$ $[M + Na]^+$: 498.21283; found: 498.21237 (observed error of -0.92 ppm is within the range of instrumental error of ±5.00 ppm).

2d: Reddish orange viscous liquid. Yield = 1.3 g (38%). R_f = 0.19 (Hexane/EtOAc 7:3). ^{1}H NMR (400 MHz, $CDCl_3$): δ = 7.93 – 7.90 (m, 2H), 7.70 (d, *J* = 7.6 Hz 1H), 7.54 – 7.39 (m, 3H), 7.43 – 7.39 (m, 2H), 7.36 – 7.31 (m, 1H), 4.23 (q, *J* = 7.1 Hz, 2H), 3.53 (t, *J* = 7.2 Hz, 2H), 1.40 (s, 18H). ^{13}C NMR [100.5 MHz, $CDCl_3$] δ 152.82, 150.45, 137.49, 131.52, 131.16, 131.02, 129.08, 127.52, 123.03, 115.46, 82.09 (d, *J* = 7.3 Hz), 67.55 (d, *J* = 6.7 Hz), 32.73 (d, *J* = 8.0 Hz), 29.77 (d, *J* = 4.2

Hz). HRMS (ESI, m/z) calculated for $C_{22}H_{31}N_2O_4PNa$ $[M + Na]^+$: 441.19137; found: 441.19107 (observed error of -0.67 ppm is within the range of instrumental error of ±5.00 ppm).

3b: Reddish orange semisolid. Yield = 0.11 g (96%). ^{1}H NMR (400 MHz, CD_3OD): δ = 9.27 (br, 1H), 7.91 (d, *J* = 6.9 Hz, 2H), 7.64 (d, *J* = 8.0 Hz, 1H), 7.55 – 7.45 (m, 4H), 7.26 (d, *J* = 8.3 Hz, 1H), 7.06 (t, *J* = 8.2 Hz, 1H), 4.43 (t, *J* = 5.1 Hz, 2H), 4.39 – 4.37 (m, 2H). ^{13}C NMR [100.5 MHz, CD_3OD] δ 157.72, 154.39, 143.83, 133.81, 132.08, 130.21, 123.98, 122.57, 117.84, 116.57, 70.48 (d, *J* = 7.7 Hz), 66.06 (d, *J* = 5.4 Hz). HRMS (ESI, m/z) calculated for $C_{14}H_{14}N_2O_5P$ $[M - H]^-$: 321.06458; found: 321.06483 (observed error of 0.77 ppm is within the range of instrumental error of ±5.00 ppm).

3c in its triethyl ammonium salt: Orange solid. Yield = 0.77g (94%). Mp: 139-141°C. ^{1}H NMR (CD_3OD, 400 MHz): δ = 8.58 (dd, *J* = 8.3, 1.1 Hz, 1H), 7.90 – 7.82 (m, 3H), 7.49 – 7.46 (m, 1H), 7.36 (d, *J* = 8.0 Hz, 1H), 7.24 – 7.19 (m, 1H), 4.54 (d, *J* = 6.1 Hz, 2H), 3.17 (q, *J* = 7.3 Hz, 6H), 2.41 (s, 3H), 2.35 (s, 3H), 1.28 (t, *J* = 7.3 Hz, 9H). ^{13}C NMR [100.5 MHz, CD_3OD] δ 169.94 (d, *J* = 9.1 Hz), 152.27, 142.33, 141.41, 138.92, 137.07, 133.06, 131.83, 127.02, 125.30, 121.50, 120.88, 118.24, 65.71 (d, *J* = 4.7 Hz), 47.71, 19.94, 19.86, 9.16. HRMS (ESI, m/z) calculated for $C_{16}H_{17}N_3O_5P$ $[M – C_6H_{17}N(TEA)]^-$: 362.09113; found: 362.09140 (observed error of 0.74 ppm is within the range of instrumental error of ±5.00 ppm).

3d in its triethyl ammonium salt: Reddish orange solid. Yield = 0.59g (51%). Mp: 130-132 °C. ^{1}H NMR (CD_3OD, 400 MHz): δ = 7.94 – 7.92 (m, 2H), 7.67 (dd, *J* = 8.1, 1.2 Hz, 1H), 7.56 – 7.49 (m, 4H), 7.43 (td, *J* = 7.4, 1.3 Hz, 1H), 7.32 – 7.29 (m, 1H), 4.14 (dd, *J* = 14.0, 7.3 Hz, 2H), 3.51 (t, *J* = 7.4 Hz, 2H), 3.16 (q, *J* = 7.3 Hz, 6H), 1.28 (t, *J* = 7.3 Hz, 9H). ^{13}C NMR [100.5 MHz, CD_3OD] δ 154.31, 151.69, 139.79, 132.72, 132.41, 132.24, 130.31, 128.36, 124.00, 116.18, 67.24, 59.54, 34.02, 8.12. HRMS (ESI, m/z) calculated for $C_{14}H_{14}N_2O_4P$ $[M - C_6H_{16}N(TEA)]^-$: 305.06967; found: 305.06991 (observed error of 0.13 ppm is within the range of instrumental error of ±5.00 ppm).

B) Triphosphate formation: The triethylammonium salt of monophosphate, **3b, 3c, 3d** (1 eq.) was converted into its tributylammonium salt through the addition of tributylamine (3.3 eq.) in dry MeOH. Triethylamine and MeOH were removed through rotary evaporation. The tributylammonium salt was dissolved in dry DMF, a solution of 1,1´-carbonyldiimidazole (6.3 eq.) in dry DMF was added under Ar atmosphere with stirring and then kept at room temperature for 16 h to proceed the reaction. Excess of 1,1´-carbonyldiimidazole was destroyed by the addition of dry MeOH (0.25 eq.) and stirring for 1hr. This solution was then added dropwise with stirring to a solution of the tributylammonium salt of pyrophosphate in dry DMF. After reacting overnight at room temperature, the mixture was cooled to 0°C in an ice bath. Cold water (4°C) was added with stirring and the pH was brought to 7.5 using 1M NaOH. The reaction mixture was extracted with ether and H_2O; the aqueous phase was evaporated with EtOH at 30°C and dried. The residue was dissolved in 0.2 M

triethylammonium hydrogencarbonate , applied to a DEAE-Sephadex A-25 column (2.5 × 30 cm, 20 g) and eluted with a linear gradient (0.2–1.0 M; total volume: 1 L) of triethylammonium hydrogencarbonate at 4°C. The product eluted in the 0.67–0.86 M range was collected and evaporated with EtOH several times to remove triethylammonium hydrogencarbonate. The obtained residue of product was converted into its sodium salt using 1M NaI in acetone and freeze dried.

4b as sodium salt: Reddish orange solid. Yield = 0.05 g (44%). Mp 161-163 °C (color changes from reddish orange to dark brown at 110 °C). ^{1}H NMR (D_2O, 400 MHz): δ = 7.27 (d, *J* = 6.6 Hz, 2H), 7.06 – 7.02 (m, 5H), 6.86 (d, *J* = 7.0 Hz, 1H), 6.69 (t, *J* = 6.6 Hz, 1H), 4.56 (m, 2H), 4.48 (m, 2H). ^{13}C NMR [100 MHz, D_2O (CD_3OD)] δ 156.22, 153.33, 142.86, 134.54, 132.67, 130.48, 123.58, 122.92, 118.18, 116.19, 70.16 (d, *J* = 7.9 Hz), 65.71 (d, *J* = 5.2 Hz). ^{31}P NMR [160 MHz, D_2O (H_3PO_4)] δ -10.89 – -11.20 (m, 2P), -23.03 – -23.19 (m, 1P). HRMS (ESI, m/z) calculated for $C_{14}H_{14}N_2O_{11}Na_4P_3$ $[M + H]^+$: 570.93957; found: 570.93993 (observed error of 0.62 ppm is within the range of instrumental error of ±5.00 ppm). RP-HPLC [Column - CN-80Ts, 4.6 × 250 mm (TOSOH); Eluent - CH_3CN/0.1M aq. NaPi(pH 6.5); flow rate – 0.5mL/min] retention time = 55.01.

4c as sodium salt : Orange solid. Yield = 0.46 g (95%). Mp 168-170 °C (color changes from orange to dark brown at 118 °C). ^{1}H NMR (D_2O, 400 MHz): δ = 7.95 (d, *J* = 7.1 Hz, 1H), 7.76 – 7.68 (m, 3H), 7.63 – 7.59 (m, 1H), 7.45 – 7.40 (m, 2H), 4.69 (d, *J* = 7.4 Hz, 2H), 2.39 (s, 3H), 2.36 (s, 3H). ^{13}C NMR [100 MHz, D_2O (CD_3OD)] δ = 170.93 (d, *J* = 9.6 Hz), 151.35, 143.78, 143.16, 139.35, 134.64, 133.11, 131.58, 127.47, 125.56, 124.48, 120.54, 118.18, 65.73 (d, *J* = 5.6 Hz), 20.03, 19.92. ^{31}P NMR [160 MHz, D_2O (H_3PO_4)] δ -10.90 (d, 1P, *J* = 18.6 Hz), -12.48 (d, 1P, *J* = 19.3 Hz), -23.06 (t, 1P, *J* = 17.8 Hz). HRMS (ESI, m/z) calculated for $C_{16}H_{17}N_3O_{11}Na_4P_3$ $[M + H]^+$: 611.96612; found: 611.96757 (observed error of 2.36 ppm is within the range of instrumental error of ±5.00 ppm). RP-HPLC [Column - CN-80Ts, 4.6 × 250 mm (TOSOH); Eluent - CH_3CN/0.1M aq. NaPi (pH 6.5); flow rate – 0.5mL/min] retention time = 76.68.

4d as sodium salt: Dark orange solid. Yield = 0.181 g (64%). Mp 153-155 °C (color changes from reddish orange to dark brown at 110 °C). ^{1}H NMR (D_2O, 400 MHz): δ = 1H NMR (400 MHz, D_2O) δ 7.96 – 7.93 (m, 2H), 7.64 – 7.59 (m, 3H), 7.56 – 7.52 (m, 2H), 7.44 – 7.41 (m, 1H), 4.24 (q, *J* = 8.0 Hz, 2H), 3.48 (t, *J* = 6.9 Hz, 2H). ^{13}C NMR [100 MHz, D_2O (CD_3OD)] δ = 153.31, 151.51, 138.15, 132.69, 132.60, 130.51, 128.75, 123.67, 116.61, 68.12 (d, *J* = 6.1 Hz), 32.82 (d, *J* = 6.8 Hz). ^{31}P NMR [160 MHz, D_2O (H_3PO_4)] δ -10.71 – -11.19 (m, 2P), -23.28 (t, 1P, *J* = 19.6 Hz). HRMS (ESI, m/z) calculated for $C_{14}H_{14}N_2O_{10}Na_4P_3$ $[M + H]^+$: 554.94466; found: 554.94501 (observed error of 0.63 ppm is within the range of instrumental error of ±5.00 ppm). RP-HPLC [Column - CN-80Ts, 4.6 × 250 mm (TOSOH); Eluent - CH_3CN/0.1 M aq. NaPi (pH 6.5); flow rate – 0.5 mL/min] retention time = 73.09.

Acknowledgements

Authors thank the Research Foundation for Opto-Science and Technology for the financial support.

References

1 R. D. Vale, *Cell*, 2003, **112**, 467–480.

2 R. D. Vale, *Science*, 2000, **288**, 88–95.

3 G. D. Bachand, N. F. Bouxsein and V. Vandelinder, 2014, **6**, 163–177.

4 N. V Delrosso and N. D. Derr, *Curr. Opin. Biotechnol.*, 2017, **46**, 20–26.

5 M. Schliwa and G. Woehlke, *Nature*, 2003, **422**, 759–765.

6 A. Goel and V. Vogel, *Nat. Nanotechnol.*, 2008, **3**, 465–475.

7 T. Korten, A. Mansson and S. Diez, *Curr. Opin. Biotechnol.*, 2010, **21**, 477–488.

8 L. Chen, M. Nakamura, T. D. Schindler, D. Parker and Z. Bryant, *Nat. Nanotechnol.*, 2012, **7**, 252–256.

9 H. Higuchi, E. Muto, Y. Inoue and T. Yanagida, *Proc. Natl. Acad. Sci. U. S. A.*, 1997, **94**, 4395–4400

10 H. Hess, J. Clemmens, D. Qin, J. Howard, V. Vogel, *Nano Lett.*, 2001, **1**, 235–239.

11 D. Wu, R. Tucker and H. Hess, *IEEE Trans. Adv. Packag.*, 2005, **28**, 594–599.

12 T. Kamei, T. Fukaminato and N. Tamaoki, *Chem. Commun.*, 2012, **48**, 7625-7627.

13 N. Perur, M. Yahara, T. Kamei and N. Tamaoki, *Chem. Commun. (Camb).*, 2013, **49**, 9935–9937.

14 P. Y. Bolinger, D. Stamou and H. Vogel, *Angew. Chemie - Int. Ed.*, 2008, **47**, 5544–5549.

15 C. V. Rao and A. P. Arkin, *Annu. Rev. Biomed. Eng.*, 2001, **3**, 391–419.

16 E. Thedinga, N. Karim, T. Kraft and B. Brenner, *J. Muscle Res. Cell Motil.*, 1999, **20**, 785–796.

17 F. Von Wegner, S. Schurmann, R. H. A. Fink, M. Vogel and O. Friedrich, *IEEE Trans. Med. Imaging*, 2009, **28**, 1632–1642.

18 S. J. Kron and J. a Spudich, *Proc. Natl. Acad. Sci. U. S. A.*, 1986, **83**, 6272–6276.

19 Y. Y. Toyoshima, S. J. Kron, E. M. McNally, K. R. Niebling, C. Toyoshima and J. A. Spudich, *Nature*, 1987, **328**, 536–539.

20 R. Cooke and W. Bialek, *Biophys. J.*, 1979, **28**, 241–258.

21 H. E. Huxley, *Nature*, 1973, **243**, 445–449.

22 R. Cooke and K. C. Holmes, *Crit Rev Biochem Mol Biol*, 1986, **21**, 53-118.

23 A. G. Szent-Györgyi, *J. Gen. Physiol.*, 2004, **123**, 631–641.

24 A. M. Gordon, E. Homsher and M. Regnier, *Physiol. Rev.*, 2000, **80**, 853–924.

25 R. Stehle, J. Solzin, B. Iorga and C. Poggesi, *Pflugers Arch. Eur. J. Physiol.*, 2009, **458**, 337–357.

26 C. Hoppmann, P. Schmieder, P. Domaing, G. Vogelreiter, J. Eichhorst, B. Wiesner, I. Morano, K. Rück-Braun and M. Beyermann, *Angew. Chemie - Int. Ed.*, 2011, **50**, 7699–7702.

27 I. Rayment, W. R. Rypniewski, K. Schmidt-Base, R. Smith, D. R. Tomchick, M. M. Benning, D. A. Winkelmann, G. Wesenberg and H. M. Holden, *Science*, 1993, **261**, 50–58.

28 I. Rayment, H. Holden, M. Whittaker, C. Yohn, M. Lorenz, K. Holmes and R. Milligan, *Science*, 1993, **261**, 58–65.

29 A. J. Fisher, C. A. Smith, J. B. Thoden, R. Smith, K. Sutoh, H. M. Holden and I. Rayment, *Biochemistry*, 1995, **34**, 8960–8972.

30 H. D. White, B. Belknap and W. Jiang, *J. Biol. Chem.*, 1993, **268**, 10039–10045.

31 E. Pate, K. Franks-Skiba, H. White and R. Cooke, *J. Biol. Chem.*, 1993, **268**, 10046–10053.

32 J. C. Grammer, H. Kuwayama and R. Yount G, *Biochemistry*, 1993, **32**, 5725–5732.

33 Kay L. Nakamaye, James A. Wells, Robert L. Bridenbaugh, Yoh Okamoto and Ralph G. Yount, *Biochemistry*, 1985, **24**, 5226-5235.

34 S. S. Margossian and S. Lowey, *Methods Enzymol.*, 1982, **85**, 55–71.

35 J. D. Pardee and J. Aspudich, *Methods Enzymol.*, 1982, **85**, 164–181.

36 S. J. Kron, Y. Y. Toyoshima, T. Q. P. Uyeda and J. A. Spudich, *Methods Enzymol.*, 1991, **196**, 399–416.

37 E. Meijering, O. Dzyubachyk and I. Smal, *Methods Enzymol.*, 2012, **504**, 183–200.

38 A. Szent-Gyorgyi, *Biol. Bull.*, 1949, **96**, 140–161.